iScience

CellPress
OPEN ACCESS

Article

Heterotypic cell-in-cell structures between cancer and NK cells are associated with enhanced anticancer drug resistance

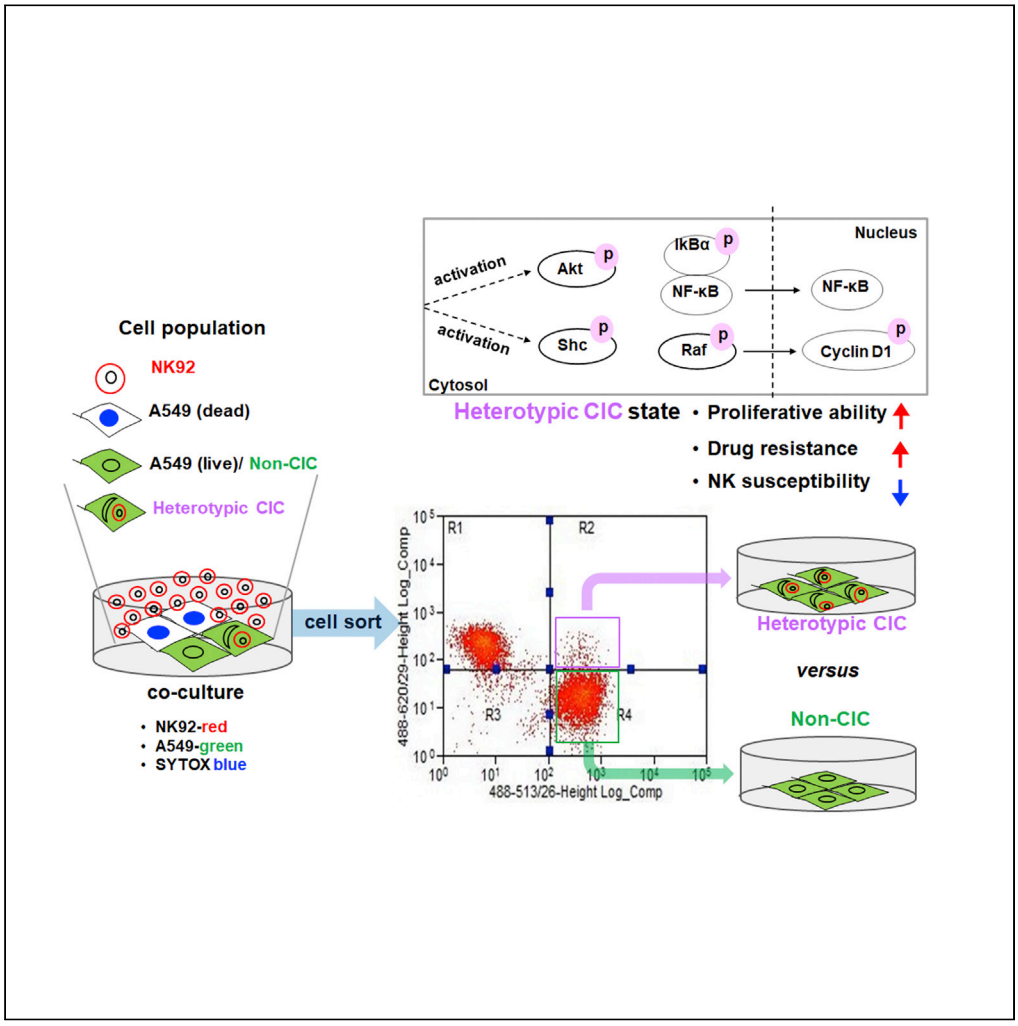

Yun-Jeong Choe, Jin Young Min, Hyunseong Lee, ..., Tae-Don Kim, Kwan Soo Hong, Eun Hee Han

heh4285@kbsi.re.kr

Highlights

Conformation of heterotypic CIC structures formed between cancer and NK cells

Heterotypic CICs exhibit a higher proliferative ability than non-CIC cells

Heterotypic CICs are associated with NK susceptibility

Heterotypic CICs are involved in anticancer drug resistance

Choe et al., iScience 25, 105017
September 16, 2022
https://doi.org/10.1016/j.isci.2022.105017

iScience

CellPress
OPEN ACCESS

Article

Heterotypic cell-in-cell structures between cancer and NK cells are associated with enhanced anticancer drug resistance

Yun-Jeong Choe,[1,9] Jin Young Min,[1,2,9] Hyunseong Lee,[1] Sang-Yeop Lee,[1] Joseph Kwon,[3] Hye-Jin Kim,[4] Jangho Lee,[5] Hyun Min Kim,[1] Hye Sun Park,[1] Mi Young Cho,[1] Ju-Yong Hyun,[1] Hye Min Kim,[1,6] Yong-Ho Chung,[1,8] Sang Keun Ha,[5,6] Hye Gwang Jeong,[2] Inpyo Choi,[6,7] Tae-Don Kim,[6,7] Kwan Soo Hong,[1,8] and Eun Hee Han[1,6,10,*]

SUMMARY

The heterotypic CIC structures formed of cancer and immune cells have been observed in tumor tissues. We aimed to assess the feasibility of using heterotypic CICs as a functional biomarker to predict NK susceptibility and drug resistance. The heterotypic CIC-forming cancer cells showed a lower response to NK cytotoxicity and higher proliferative ability than non-CIC cancer cells. After treatment with anticancer drugs, cancer cells that formed heterotypic CICs showed a higher resistance to anticancer drugs than non-CIC cancer cells. We also observed the formation of more CIC structures in cancer cells treated with anticancer drugs than in the non-treated group. Our results confirm the association between heterotypic CIC structures and anticancer drug resistance in CICs formed from NK and cancer cells. These results suggest a mechanism underlying immune evasion in heterotypic CIC cancer cells and provide insights into the anticancer drug resistance of cancer cells.

INTRODUCTION

The formation of cell-in-cell (CIC) structures, colloquially known as cell cannibalism, is a unique pathological phenomenon defined as the presence of one or more cells inside a host cell, resulting in the death of the cells present inside (Wang et al., 2020; Huang et al., 2015a). CICs have been observed in various types of human tumors and can be classified into different subtypes: Homotypic CICs (entosis) formed between tumor cells and heterotypic CICs formed via internalization of immune cells into tumor cells (Huang et al., 2015b, 2020). Over the past decade, studies on the formation of CICs between immune cells and tumor cells have been performed to investigate in detail the CIC mechanisms and cell fate (Huang et al., 2015a, 2020). The immune cells internalized in tumor cells could include T lymphocytes and natural killer (NK) cells (Caruso et al., 2012; Sierro et al., 2015). The engulfed cells are destroyed after being trapped in vacuoles, thus triggering apoptosis (Wang and Wang, 2013).

Recent advances have shown that CIC structures play important roles not only in tumor evolution and genome instability but also in embryonic development and immune homeostasis (Fais and Overholtzer, 2018; Schenker et al., 2017). Therefore, heterotypic CICs might serve as a mechanism of immune evasion to promote cancer progression (Zhang et al., 2019). Ruan et al., reported an unusual case of a patient with breast cancer whose tumor was highly heterogeneous and contained a considerable rate of complex CIC structures (~6%), a phenomenon that may be related to active cell proliferation and unfavorable prognosis (Ruan et al., 2019). However, the contribution of heterotypic CICs to NK cytotoxicity and anticancer drug resistance has not yet been established.

Cancer immunotherapy and chemotherapy have been used extensively in tumor treatment, including both systemic and local treatment (Zhang et al., 2020). The resistance of cancer cells to anticancer drugs is an important cause of treatment failure (Zhang et al., 2020). The combination of chemotherapy or molecular targeted drugs and immunotherapy drugs is emerging as a promising therapeutic strategy to prevent tumor recurrence. However, non-responders to immunotherapy and drug resistance to chemotherapy remain major challenges. Overcoming these challenges is necessary to achieve long-lasting and effective

[1]Research Center for Bioconvergence Analysis, Korea Basic Science Institute, Cheongju 28119, South Korea

[2]Department of Toxicology, College of Pharmacy, Chungnam National University, Daejeon 34134, South Korea

[3]Research Center for Materials Analysis, Korea Basic Science Institute, Daejeon 34133, South Korea

[4]Tomocube, Inc., Daejeon 34051, South Korea

[5]Research Division of Food Functionality, Korea Food Research Institute, Jeollabuk-do 55365, South Korea

[6]Korea University of Science and Technology (UST), Daejeon 34113, Republic of Korea

[7]Immunotherapy Research Center, Korea Research Institute of Bioscience and Biotechnology, Yuseong-gu, Daejeon 34141, Republic of Korea

[8]Graduate School of Analytical Science and Technology, Chungnam National University, Daejeon 34134, South Korea

[9]These authors contributed equally

[10]Lead contact

*Correspondence: heh4285@kbsi.re.kr

https://doi.org/10.1016/j.isci.2022.105017

cancer treatment and to prevent cancer recurrence Zhang et al. (2019); Zhang et al. (2020)]. Mechanisms to stratify immunotherapy non-responders and inducing anticancer drug resistance have been extensively investigated but remain to be fully characterized.

This study aims to explore the feasibility of using heterotypic CICs as a functional biomarker to predict NK susceptibility and drug resistance in solid cancer cell lines including A549, PLC/PRF/5, A431, and A375SM. We propose that it will be important to utilize our knowledge of heterotypic CICs to predict immunotherapeutic non-responders and develop therapeutic applications to overcome anticancer drug resistance.

RESULTS

Conformation of heterotypic CIC structures formed between cancer and NK cells

NK-92 cells were co-cultured with the A549 human non-small-cell lung cancer (NSCLC) cell line to conduct CIC imaging experiments. For time-lapse microscopic imaging, the effector cells (suspended NK-92) and epithelial target tumor cells (attached A549) were stained with calcein green and calcein red-orange, respectively, before starting co-culture at an effector:target (E:T) ratio of 4:1 for 5 h A549 cells were treated with NK-92 cells, and then SYTOX blue for dead cell staining was added to the culture medium. As expected, A549 cells killed by NK cells were imaged with green to blue fluorescence (Figure S1 and Video S1). During this imaging experiment, a heterotypic CIC phenomenon was unexpectedly observed (Figure 1A and Video S2). To avoid error of fluorescence labeling, optical diffraction tomography (ODT) was performed using an HT-2H equipment together with TEM imaging confirmation. ODT enables imaging of heterotypic CICs by measuring three-dimensional (3D) refractive index (RI) of microscopic objects in a label-free or fluorescence-dependent manner in wide area of cultured live cells. The A549 and NK-92 cells were confirmed to have different RI values (Figure S2A) and the presence of heterotypic CIC structures was confirmed after co-culture of non-labeled A549 and NK-92 cells via ODT imaging (Figure 1B andVideo S3). Heterotypic CIC formation was also confirmed when NK-92 cells were stained with calcein green AM and then co-cultured with A549 cells at an E:T ratio of 4:1 (Figure 1C and Video S4). Cellular TEM images also revealed that heterotypic CICs were formed from the culture of A549 and NK-92 cells (Figure 1D). Accordingly, we concluded that heterotypic CICs were formed during the co-culture of A549 and NK-92 cells.

Next, we quantitatively analyzed the structure of heterotypic CICs by flow cytometry analysis. Briefly, NK-92 stained with anti-CD45-PE and A549 cells stained with CellTracker CMFDA green were co-cultured to allow the formation of heterotypic CIC structures, and the subsequent cell populations were analyzed by stained fluorescence (He et al., 2015). Cell suspensions analyzed by flow cytometry were prepared by complete trypsinization following removal of floating NK-92 cells that had not bound to or infiltrated inside A549 cells.

Heterotypic CICs were defined as double-positive, whereas those that were single positive were defined as A549 cells not forming CIC structure (non-CICs). Measurement of heterotypic CIC populations revealed that A549 cells could form heterotypic CICs with NK-92 cells at a rate of approximately 3–8% after co-culture for 3–8 h (Figures 1E and 1F).

Heterotypic CIC structures have been observed following co-culture of various solid tumor and immune cells, and it is known that internalized immune cells undergo cell death (He et al., 2015; Almangush et al., 2020). The cellular morphology of heterotypic CICs in CMFDA green images showed black holes in which NK-92 cells were present (Figures S2B and S2C) and internal NK-92 cells were observed to undergo cell death by TEM imaging (Figure S2D). However, in the ODT imaging, images of NK-92 cells entering and killing A549 cells were also taken (Video S5). This phenomenon fell outside the scope of this study and was therefore not followed up.

Heterotypic CIC population exhibits a lower response to NK cytotoxicity and higher proliferative ability than non-CIC cells

Recent studies have shown that heterotypic CIC structures of immune and cancer cells are associated with an immune evasion mechanism that promotes cancer progression, tumor evolution and genomic instability and is associated with an unfavorable prognosis in cancer patients (Caruso et al., 2012; Sierro et al., 2015; Fais and Overholtzer, 2018; Zhang et al., 2019; Ruan et al., 2019). Until now, many studies on heterotypic CICs between immune cells and tumor cells have reported this phenomenon; however, direct studies on the difference between CIC and non-CIC cells are lacking. Therefore, it would be interesting to investigate

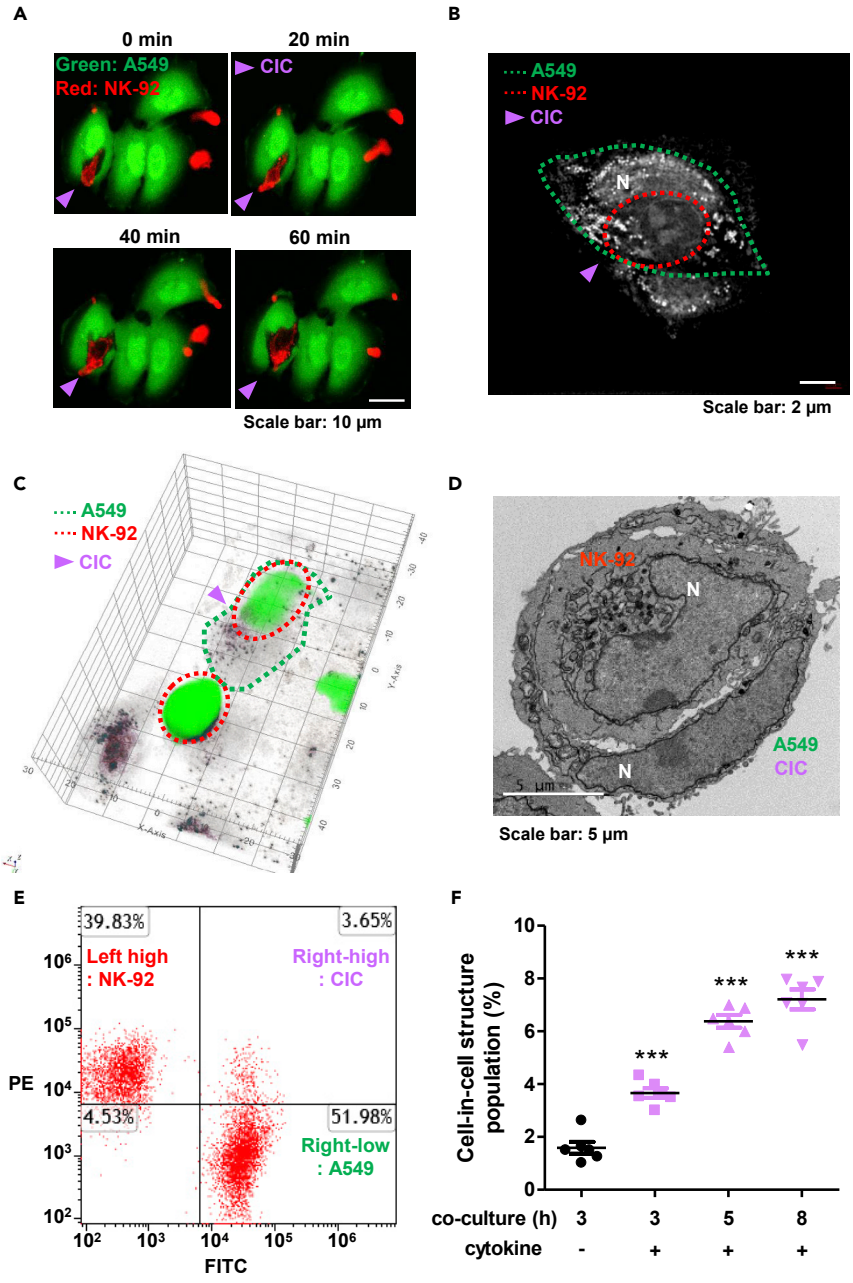

Figure 1. Analysis of heterotypic CIC structures formed between A549 and NK-92 cells

(A) Time-lapse confocal images of heterotypic CICs. A549 cells were stabilized overnight on a confocal slide and then stained with calcein green am. NK-92 cells stained with calcein red-orange am were added to the slide (E:T ratio = 4:1) and then imaged for a total of 1 h. Arrows indicate heterotypic CIC structure. Scale bar = 10 μm.

(B) Cellular ODT images of live cultured heterotypic CICs for label-free measurements. N indicates the nucleus.

(C) 3D rendering image merged with fluorescence of heterotypic CIC. The green line marks the outer cell (A549); red line indicates the internalized cell (NK-92); purple arrows indicate heterotypic CIC structures.

(D) A representative TEM image of heterotypic CIC with NK-92 cells inside A549 cells. N indicates the nucleus. Scale bar: 5 μm.

(E) Flow cytometry analysis for heterotypic CICs. Image shows the % of the total cell population. Left-high = CD45-PE labeled NK-92, right-high = heterotypic CIC, and right-high = CMFDA green labeled A549 (non-CIC).

(F) Graph showing the quantification results of heterotypic CIC population (double-positive, right-high) for 3, 5, and 8 h of co-culture in the presence of cytokine (IL-2). Statistical analysis included one-way ANOVAfollowed by Newman–Keuls multiple comparison test (***, $p<0.001$). The experiment was performed independently 6 times.

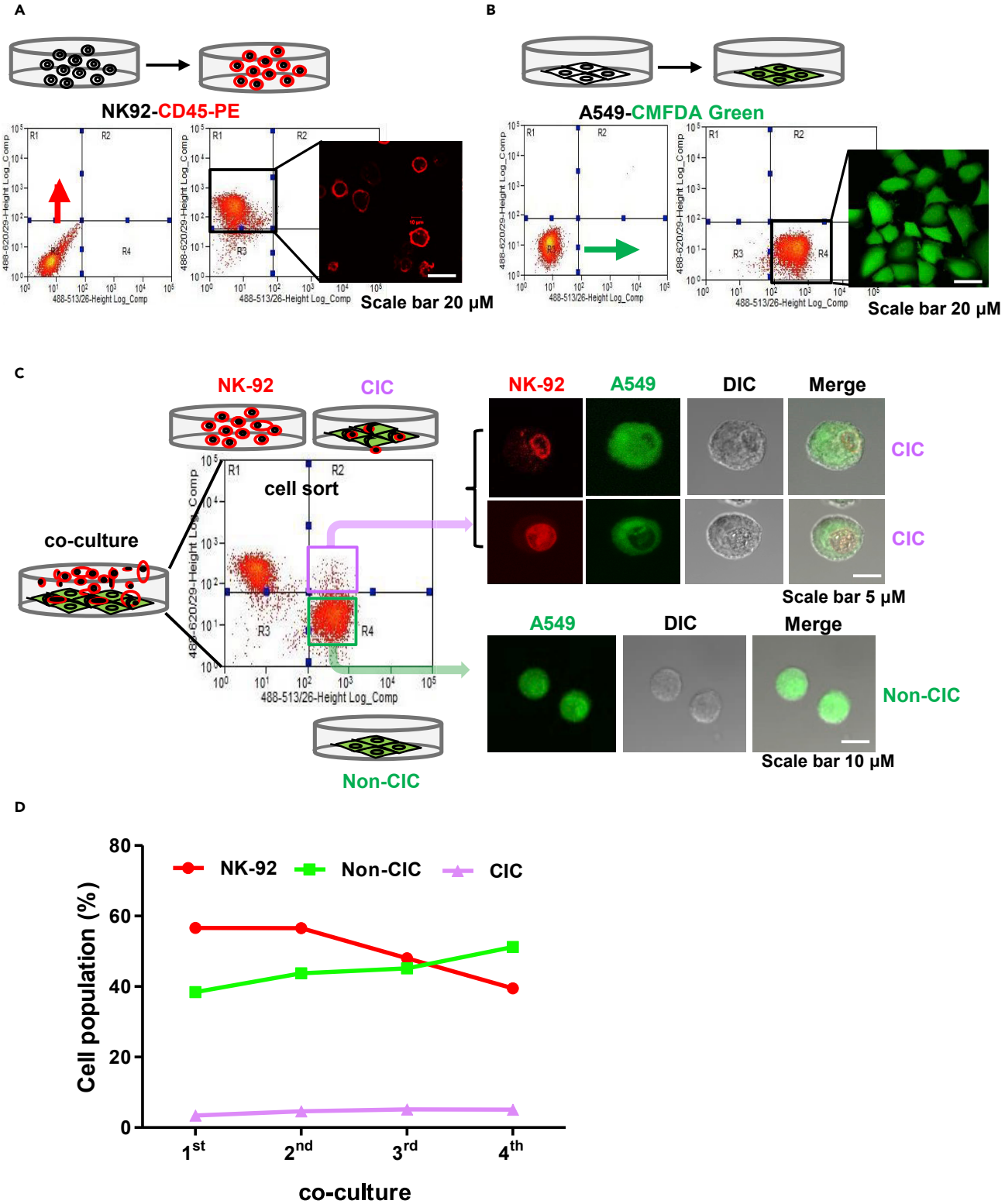

Figure 2. Cell sorting procedure and heterotypic CIC structure formation pattern analysis

NK-92 and A549 cells were labeled with CD45-PE and CMFDA green, respectively, and positive cells were distributed in left-high (A) and right-low (B) when flow cytometry analysis was performed. Representative fluorescence images of single positive cells are presented.

Figure 2. *Continued*

(C) After 4 h of co-culture of the two fluorescently labeled cells, heterotypic CIC (double-positive, right-high) and non-CIC (single positive, right-low) cancer cells were separated by a cell sorter. Representative fluorescence images of sorted heterotypic CICs and non-CICs are presented.

(D) Flow cytometry analysis of the heterotypic CIC structure formation pattern. Starting with the first heterotypic CIC classified after co-culture with A549 and NK-92, heterotypic CIC was repeatedly classified 4 times by co-culture with NK-92. The red line indicates the population of NK-92 cells, the green line indicates non-CICs, and the purple line indicates the population of heterotypic CICs.

the differences between cells that form heterotypic CICs and non-CICs, and to examine the characteristics of heterotypic CIC cell populations. In this study, two types of cells (double-positive or single-positive fluorescence cells) were isolated using a cell sorter to conduct additional studies on the differences between heterotypic CIC and non-CIC cancer cells. After staining of NK-92 and A549 cells as shown in Figure 1E, heterotypic CIC cells were separated into double-positive fluorescent cells and non-CIC cells into single positive fluorescent cells (Figures 2A and 2B). As one of the methods to determine the difference between CICs and non-CICs, we investigated whether the ratio of heterotypic CIC-inducing cancer cells was increased by repeatedly sorting heterotypic CICs. A549 and NK-92 were co-cultured and CICs were sorted; these CICs were repeatedly co-cultured with NK-92 cells 4 times to quantify the CIC cell population. As shown in Figure 2C, the proportion of the CIC population showed a similar regardless of the number of co-cultures. Although not statistically significant, the rate of non-CIC cells not killed by NK-92 cells showed an increasing trend (Figures 2C and Video S3). Therefore, it we hypothesized that the CIC population would be more resistant to NK-92 cell-mediated cytotoxicity than non-CICs.

Measurement of the difference between non-CIC and CIC responses to NK cytotoxicity revealed that compared to non-CICs, heterotypic CIC-inducing cancer cells were not killed by NK-92 cells under the E:T ratios of 4:1 and 6:1 (Figure 3A). The heterotypic CIC-inducing cell population in the condition of 500 cells showed faster cell growth than non-CICs (Figure 3B). Furthermore, cell cycle analysis confirmed a relatively high proportion of cells in the S and G2/M compared to that in non-CICs (Figure 3C), indicating that the heterotypic CIC population progressed through the cell cycle more rapidly than non-CICs, suggesting increased cell growth.

Next, we performed foci and soft agar colony formation assays to determine whether cancer cells that induce heterotypic CICs are more likely to induce malignant transformation than non-CIC population. As shown in Figure 3D, the heterotypic CIC population showed increased foci formation compared to that by non-CICs when seeded at a density of 500 and 1000 cells. Similarly, cancer cells inducing heterotypic CICs featured an increased anchorage independent growth and invasion assay compared to that by non-CICs when seeded at densities of 5×10^4 and 1×10^5 cells (Figures 3E and 3F). These results indicate that heterotypic CICs had a higher malignant phenotype than non-CICs.

Heterotypic CICs are involved in anticancer drug resistance

Currently, chemotherapy using anticancer agents is actively used for treatment of lung cancer, but recurrence because of advanced lung cancer or drug resistance remains a major limitation of lung cancer treatment (Stewart, 2010; Vasan et al., 2019). Gao et al. showed that the A549 NSCLC cell line harbors different subpopulations, including a mesenchymal-like subpopulation characterized by increased chemo- and radiotherapy resistance (Gao et al., 2019).

In addition to the relatively malignant phenotype compared to non-CICs, we investigated the effect of the presence of heterotypic CICs in tumor tissue on anticancer drug resistance. Cisplatin, doxorubicin, gemcitabine, etoposide, and docetaxel are representative chemotherapeutic agents used to treat a wide spectrum of human cancers, including lung cancer (Ichite et al., 2009). To investigate the anticancer drug response between heterotypic CICs and non-CICs, we measured the proliferation of cells by CCK-8 assay, following the manufacturer's instructions. Cell proliferation of both populations decreased after drug administration in a dose dependent manner, but the responsiveness of heterotypic CICs was relatively lower than non-CICs (Figures 4A–4E).

To verify the correlation between CIC and drug resistance, the differences between the CIC populations were quantitatively analyzed after co-culture of NK-92 cells with surviving cells (heterotypic CIC and non-CIC, respectively) and chemotherapeutic drug treatment. Among various anticancer drugs, doxorubicin, which showed uniform proliferation changes in heterotypic CIC and non-CIC, and gemcitabine,

which showed the smallest cell viability change, were selected. To produce drug-resistant cancer cells, we treated non-CIC and heterotypic CIC populations with doxorubicin and gemcitabine, and surviving cells were defined as drug resistant. Drug treatment involved continuous exposure to doxorubicin (10 μM) and gemcitabine (10 μM) for 2 weeks. Quantitative analysis of the CIC population by co-culture with NK-92 for viable cancer cells during anticancer drug treatment, the CIC formation rate was higher in the CIC population than in the non-CICs (Figure 5A). We established an experimental approach to further investigate whether the heterotypic CIC population is associated with chemotherapy resistance. After treatment of A549 cells with low concentrations of doxorubicin (1 μM) and gemcitabine (5 μM), surviving cells were co-cultured with NK-92 cells to analyze the subsequent CIC populations. As a result, a more CIC population was observed in A549 cells treated with anticancer agents than in the control group (Figure 5B). Therefore, we concluded that heterotypic CIC-forming cancer cells would demonstrate lower anticancer drug susceptibility and higher drug resistance than non-CIC cancer cells.

To decipher the signaling mechanisms involved in cell proliferation and resistance to NK-92 cells and anticancer drug treatment of heterotypic CIC-forming cancer cells, we performed phospho-antibody arrays using 304 phospho antibodies. Phosphorylation of signaling proteins such as Cyclin D1 and Akt were increased in heterotypic CIC-forming cancer cells compared to non-CICs (Figure 5C). Functional analysis was performed using IPA (Ingenuity Systems, Redwood City, CA, USA; www.ingenuity.com) and identified networks of signaling proteins for drug resistance mechanisms of the heterotypic CIC-forming cancer cells linked to the dataset using the Ingenuity Knowledge Base (Figure 5D).

Anticancer drug resistance and heterotypic CIC structure were positively correlated in EGFR-overexpressing cancer cell lines

Small molecule and antibody inhibitors targeting the EGFR have been developed because of the role of this receptor in regulating cell growth, but many cancers are initially resistant to EGFR inhibitors or become resistant during treatment, thus, limiting the efficacy of these drugs (Tetsu et al., 2016). Currently, EGFR inhibitors are gaining considerable interest for their clinical roles in several cancers, usually as a component of combination therapy.

In addition to lung cancer cell lines, we investigated the correlation between CIC populations and drug resistance in EGFR-overexpressing cancer cell lines. Flow cytometry analysis revealed that hepatocellular carcinoma PLC/PRF/5 and epidermoid carcinoma A431 cells containing mutant p53 overexpress the EGFR protein (Figure 6A). Similarly, the PLC/PRF/5 and A431 cancer cells showed heterotypic CICs with NK-92 cells at a rate of 3.06 and 2.67%, respectively (Figures 6B and 6C). PLC/PRF/5 and A431 cells were also co-cultured with NK-92 cells after anticancer drug treatment using the same methodology as for A549 cells, and similar results were obtained. The number of heterotypic CIC cells was increased when the drug-resistant PLC/PRF/5 and A431 cancer cells were co-cultured with NK-92 cells compared to that in the control cells (Figures 6D and 6E). Therefore, a positive correlation between anticancer drug resistance and heterotypic CIC structure were also confirmed in EGFR-overexpressing cell lines.

Correlation between frequency of heterotypic CIC structures and anticancer drug resistance in human cancer organoids and *in vivo* xenograft models

It is known that multidrug resistance (MDR) in cancer cells is primarily because of overexpression of ATP-binding cassette transporters such as ABCB1 (Priya et al., 2022). To verify the correlation between the frequency of heterotypic CIC structures and drug resistance *in vivo*, reflecting the tumor microenvironment, and in a three-dimensional human cancer organoid similar to an actual tumor, an anticancer drug resistance experimental model was established using the ABCB1 gene. Human ABCB1 (hABCB1) gene was expressed in NSCLC A549 and human melanoma A375SM cells using lentivirus infection, and drug uptake resistance was confirmed using rhodamine 123 dye. As a result of analysis using confocal microscopy and flow cytometry, the intracellular uptake of rhodamine 123 was significantly reduced in hABCB1-overexpressing A549 and A375SM cells compared to the wild-type control group (Figures S4A and S4B).

Next, anticancer drug resistance to doxorubicin and paclitaxel was confirmed in NSCLC (A549 wild-type or hABCB1) and melanoma (A375SM wild-type or hABCB1) cells (Figures 7A and 7B). In addition, it was verified that the heterotypic CIC structure population increased in hABCB1-overexpressing A549 and A375SM cells compared to wild-type cells (Figure 7C). These cancer cells were injected subcutaneously into SCID mice to establish NSCLC (A549 wild-type or hABCB1) and melanoma (A375SM wild-type or hABCB1)

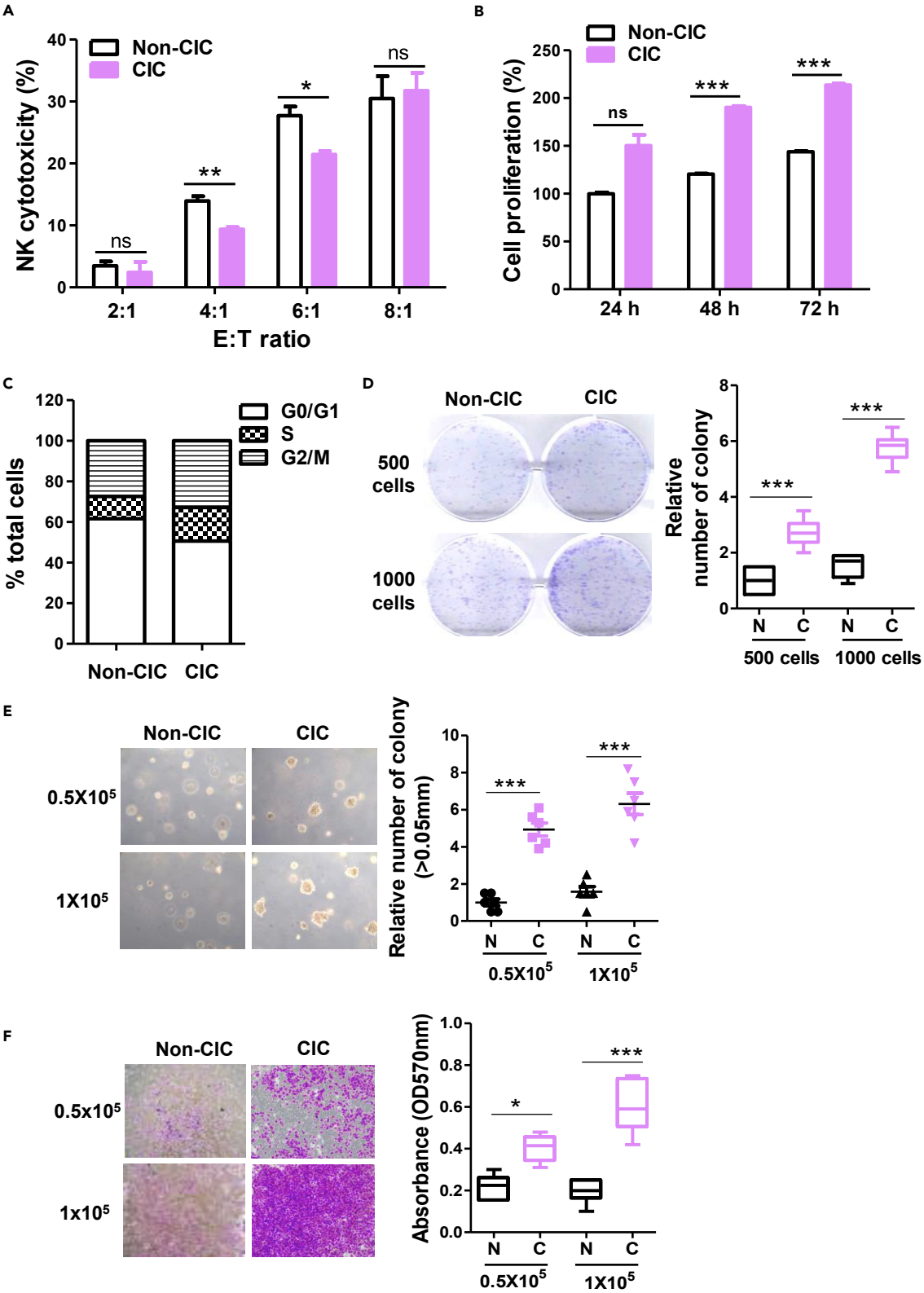
A
Non-CIC
CIC
NK cytotoxicity (%)
ns
**
*
ns
2:1
4:1
6:1
8:1
E:T ratio
B
Non-CIC
CIC
Cell proliferation (%)
ns
***
***
24 h
48 h
72 h
C
G0/G1
S
G2/M
% total cells
Non-CIC
CIC
D
Non-CIC
CIC
500 cells
1000 cells
Relative number of colony
***
***
N
C
N
C
500 cells
1000 cells
E
Non-CIC
CIC
0.5X10^5
1X10^5
Relative number of colony (>0.05mm)
***
***
N
C
N
C
0.5X10^5
1X10^5
F
Non-CIC
CIC
0.5x10^5
1x10^5
Absorbance (OD570nm)
*
***
N
C
N
C
0.5X10^5
1X10^5

Figure 3. Analysis of the difference between heterotypic CICs and non-CICs on NK cytotoxicity reactivity and effects of tumor progression

(A) Effects of heterotypic CICs and non-CICs on NK cytotoxicity. Heterotypic CICs and non-CICs were stained with calcein AM and effector NK-92 cells were added for 4hat E:T ratios of 2:1, 4:1, 6:1 and 8:1. NK cytotoxicity was analyzed by detecting the fluorescence of calcein released from the supernatant of the killed cancer cells. p values were determined by student's *t*-tests.

(B) Effects of heterotypic CICs and non-CICs on cell proliferation rate. 500 heterotypic CICs and non-CICs cells were inoculated into a 96-well plate, and cell proliferation was measured by CCK-8 assay at 24, 48, and 72 h. p values were determined by the student's *t*-tests.

(C) Effects of heterotypic CICs and non-CICs on cell cycling. Cell cycle phases (G0/G1, S, and G2/M) were measured using flow cytometry in 10,000 cells stained with Hoechst 33,342. Effects of heterotypic CIC and non-CIC on focus formation (D), anchorage independent growth (E), and invasion (F) assay. Statistical analysis included ANOVA followed by Newman–Keuls multiple comparison test. All experiments were independently performed 6 times.

*, $p<0.05$; **, $p<0.01$; ***, $p<0.001$; ns, not significant.

xenograft models. Because it was confirmed in an *in vitro* experiment that drug resistance to doxorubicin and paclitaxel was stably induced by hABCB1 overexpression, NK-92 cells were injected into the tumor to examine the heterotypic CIC structure. All tumors (A549 wild-type and hABCB1; n = 5, A375SM wild-type and hABCB1; n = 3 and n = 5) were isolated, single cells were prepared, and then red blood cells were lysed so that only cancer cells and injected NK-92 were present. After permeabilizing cells to analyze NK-92 cells present in cancer cells (heterotypic CIC structure), cancer and NK-92 cells were stained with E-cadherin and human CD45 antibody, respectively. As a result of heterotypic CIC population analysis, hABCB1 overexpressing tumors increased compared to wild-type tumors, and the A549 NSCLC model was more significant than the A375SM melanoma model (Figures 7D and S4C).

To confirm the correlation between heterotypic CIC populations and drug resistance in human tumors but not in mouse models, we established a three-dimensional tumor model by overexpressing hABCB1 in human gastric adenocarcinoma cancer organoids. After treatment with rhodamine 123 as in the *in vitro* experiment, it was confirmed that drug uptake was reduced in hABCB1-overexpressing cancer organoids (SNU-CO-1) compared to wild-type cells under a confocal microscope imaging (Figure S4D). In addition, drug resistance to doxorubicin and paclitaxel was confirmed in hABCB1-overexpressing cancer organoids (Figure 7E), and the heterotypic CIC population was also increased in hABCB1-overexpressing cancer organoids compared to wild-type cells (Figure 7F). Taken together, these results lead us to conclude that the heterotypic CIC structure of cancer cells with NK cells is strongly associated with anticancer drug resistance.

DISCUSSION

CIC structure is a term describing the phenomenon in which one or more cells becomes internalized inside a host cell, usually resulting in internal cell death; this process is coordinated by a series of key elements, including adhesion junctions, acytomyosins, and mechanical rings (Wang et al., 2020; Huang et al., 2015b; Hamann et al., 2019). CIC is prevalent in a wide range of human tumors and can be categorized into the subtypes, homotypic CICs formed by internalization between tumor cells and heterotypic CIC formed by internalization of immune cells into tumor cells (Huang et al., 2015b; Overholtzer and Wang, 2015; AbdullGaffar, 2020; Chen et al., 2013). Heterotypic CIC has also been proposed as an immune evasion mechanism that promotes cancer progression and predicts patient prognosis (Huang et al., 2020; Zhang et al., 2019; Onishi et al., 2016). The formation of these heterotypic intracellular cellular structures suggests that tumor cells may modulate the tumor microenvironment (TME) by unique mechanisms (Fais and Overholtzer, 2018; Almangush et al., 2020; Hayashi et al., 2020; Wang et al., 2019). In this study, NK-92 and A549 lung cancer cells were co-cultured, and CLSM imaging experiments and flow cytometry-based quantitative analyses were performed to identify the population of cancer cells forming heterotypic CIC structures. In addition, heterotypic CIC and non-CIC cancer cells were isolated using a flow cytometry-based cell sorter.

We explored the differences between heterotypic CIC and non-CIC populations rather than focusing on the NK-92 cells internalized within cancer cells. Analysis of the CIC population after repeated co-culture with NK-92 cells and heterotypic CIC-induced cancer cells revealed that the number of cancer cells that survived without being killed by NK-92 cells increased, despite a similar CIC ratio being produced after each co-culture. To identify the difference between heterotypic CIC and non-CIC cancer cells, the sensitivity to NK cells was measured based on NK cytotoxicity and their effects on tumorigenesis were compared. Interestingly, the heterotypic CIC population showed lower NK sensitivity and a higher malignant phenotype than non-CICs. To elucidate the reasons underlying the low NK cytotoxic reactivity in the heterotypic CIC population, further studies are needed to determine whether the expression of NK cell ligands, such as ULBP and MICA/B, is reduced. According to previous reports, heterotypic CICs were

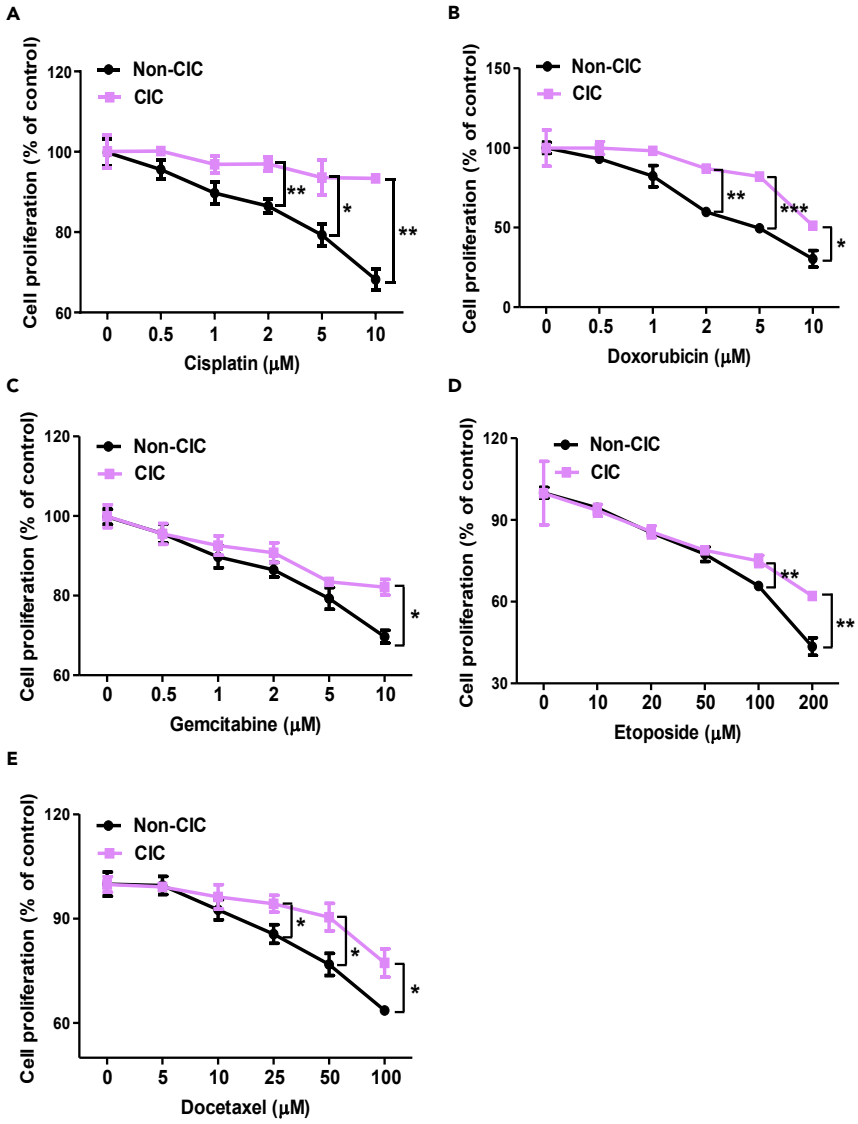

Figure 4. Analysis of the difference in anticancer drug response between heterotypic CIC and non-CIC populations

Cell proliferation of heterotypic CICs and non-CICs was measured by CCK-8 assay after treatment with various concentrations of anticancer drugs, including cisplatin (A), doxorubicin (B), gemcitabine (C), etoposide (D), and docetaxel (E). p values were determined by the student's *t*-tests. All experiments were performed in triplicate. *, $p<0.05$; **, $p<0.01$; ***, $p<0.001$.

expected to be relatively more malignant than non-CICs, although the effect on anticancer drug reactivity and drug resistance in heterotypic CIC population has not been reported yet.

We further explored the correlation between the heterotypic CIC population and anticancer drug resistance compared to that in non-CIC cancer cells. The drug reactivity was lower in heterotypic CICs than in non-CICs following treatment with various chemotherapy drugs, and a higher CIC ratio was observed in heterotypic CICs when treated with anticancer drugs. In addition, compared to the control group, A549 parental cells with anticancer drug resistance showed a higher CIC ratio when co-cultured with NK-92 cells. The reason for the high anticancer drug resistance in the heterotypic CIC population appears to be related to the increased rate of cells in the S and G2/M cell cycles, resulting in rapid proliferation.

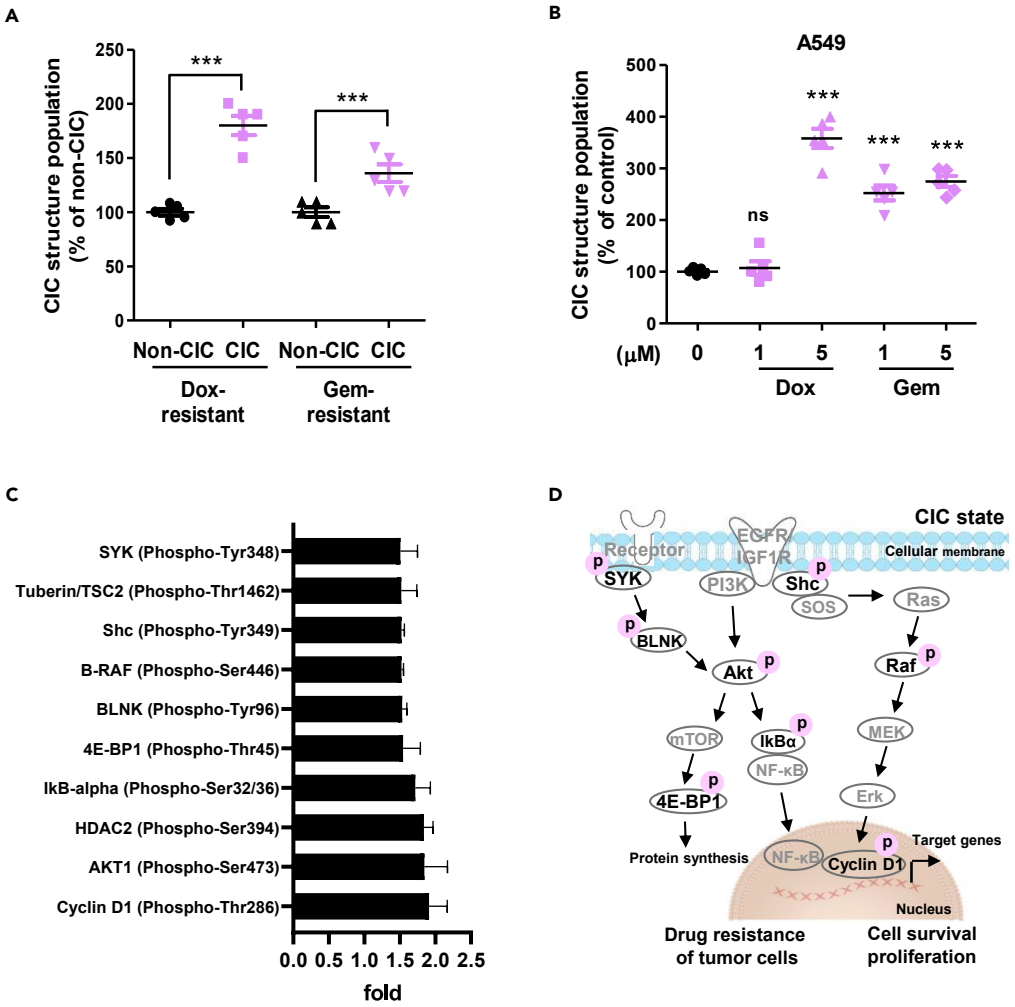

Figure 5. Analysis of heterotypic CIC structures between NK-92 and cancer cells

(A) Effects of heterotypic CIC structure formation rate by co-culture with anticancer drug (doxorubicin or gemcitabine)-resistant non-CIC or CICs and NK-92 cells.

(B) Effects of heterotypic CIC population rates by anticancer drug treatment in co-cultures NK-92 and A549 cells. A549 cells were treated with doxorubicin (1 and 5 μM) or gemcitabine (1 and 5 μM) for 24 h, and then co-cultured with NK-92 cells for 4 h to analyze the heterotypic CIC population. Dox indicates the doxorubicin; Gem indicates the gemcitabine. Statistical analysis included ANOVA followed by Newman–Keuls multiple comparison test. All experiments were performed 5 times. ***, $p<0.001$.

(C) Phospho antibody arrays for cell signaling network analysis of heterotypic CIC populations. As shown, the phosphorylation site of the signal protein increases by more than 1.5 times.

(D) Molecular signaling transduction pathways of heterotypic CIC populations. IPA analysis showing activation of signaling proteins and functional pathways associated with drug resistance of tumor cell lines in a heterotypic CIC population. Among the signaling proteins, proteins not derived from the antibody array are shown in gray. IGF1R: insulin-like growth factor 1. SYK: spleen associated tyrosine kinase. BLNK: B-Cell Linker Protein. EGFR: epidermal growth factor receptor. **RAS**: rat sarcoma viral oncogene homolog. **RAF**: proto-oncogene serine/threonine-protein kinase. **MEK**: mitogen-activated protein kinase kinase. **Erk**: mitogen-activated protein kinase. **PI3K**: phosphatidylinositol 3-kinase. **AKT**: protein kinase B. **mTOR**: mammalian target of rapamycin complex 1. 4E-BP1: 4E-binding protein 1.

The p53 protein is encoded by the cancer suppressor gene *TP53*. Its functions include regulation of the cell cycle, aging, apoptosis, repair of DNA damage caused by genotoxic agents, angiogenesis, and regulation of oxidative stress (Foulkes, 2007). Mutation of the *TP53* gene has been shown to increase the CIC phenomenon, possibly via a process associated with EGFR and integrin expression (Mackay et al., 2018). Furthermore, as EGFR inhibitors exhibit drug resistance and, thus, decrease the efficacy of anticancer drugs, we attempted to investigate the correlation between EGFR and CIC in cancer cell lines with p53 mutations

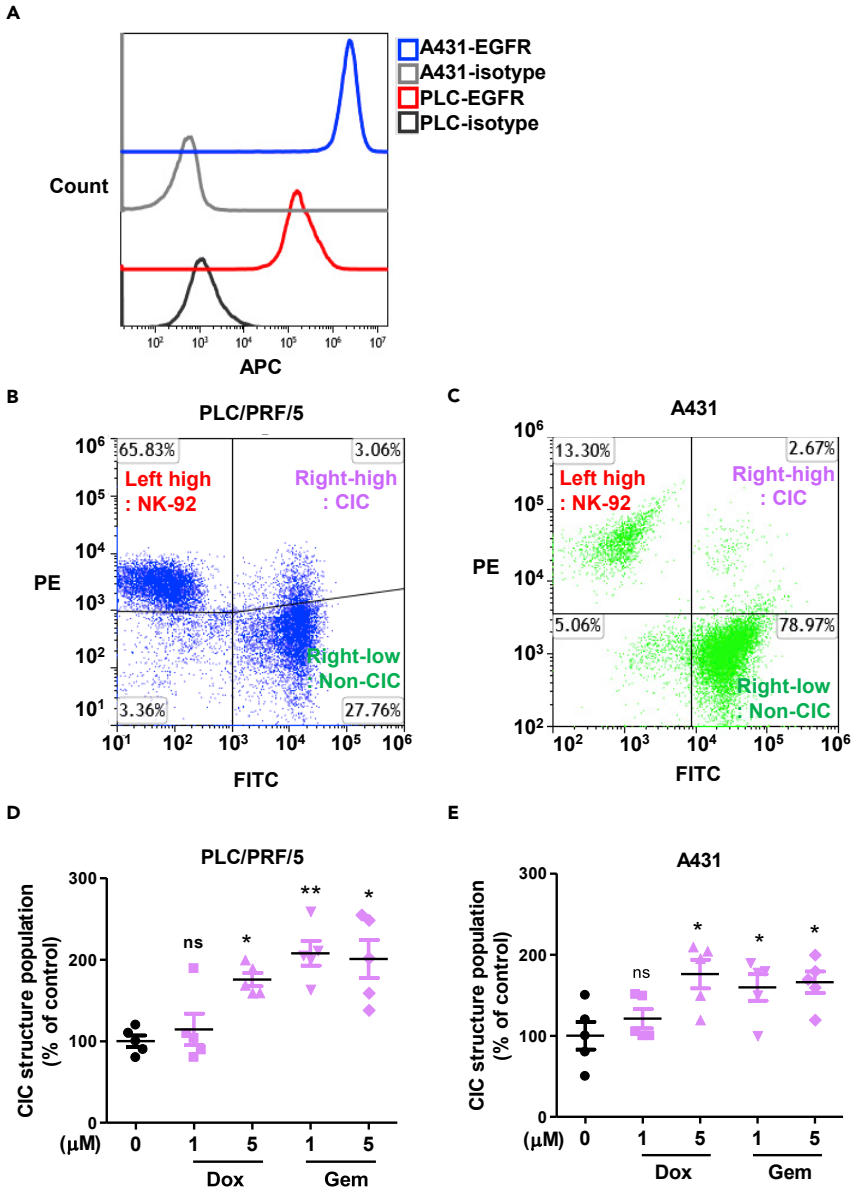

Figure 6. Analysis of heterotypic CIC structures between EGFR overexpressing cancer and NK-92 cells

(A) EGFR expression in A431 and PLC/PRF/5 cells was measured by flow cytometry after treatment with 5 μL per sample and labeling with EGFR-Alexa Fluor 647 antibody.

(B and C) Flow cytometry analysis of heterotypic CICs. Images show the % of cell population. Left-high = CD45-PE labeled NK-92, right-high = heterotypic CIC, and right-high = CMFDA green labeled PLC/PRF/5 (B) and A431 (C).

(D and E) Effects of heterotypic CIC population rate by anticancer drug treatment in co-culture with NK-92 and cancer cells. PLC/PRF/5 (D) and A431 (E) cells were treated with doxorubicin (1 and 5 μM) or gemcitabine (1 and 5 μM) for 24 h, and then co-cultured with NK-92 cells for 4 h to analyze the heterotypic CIC population. Dox indicates the doxorubicin; Gem indicates the gemcitabine. Statistical analysis included ANOVA followed by Newman–Keuls multiple comparison test. All experiments were performed 5 times. *, $p<0.05$; **, $p<0.01$; ns, not significant.

and high EGFR expression. In the PLC/PRF/5 and A431 cell lines, a heterotypic CIC population was observed following co-culture with NK-92 cells, and a higher CIC ratio was observed in anticancer drug resistant cells than in the control group. Furthermore, we established a hABCB1 gene overexpression model to confirm the correlation between the frequency of heterologous CIC structures and anticancer drug resistance in human cancer organoids and *in vivo* xenograft models.

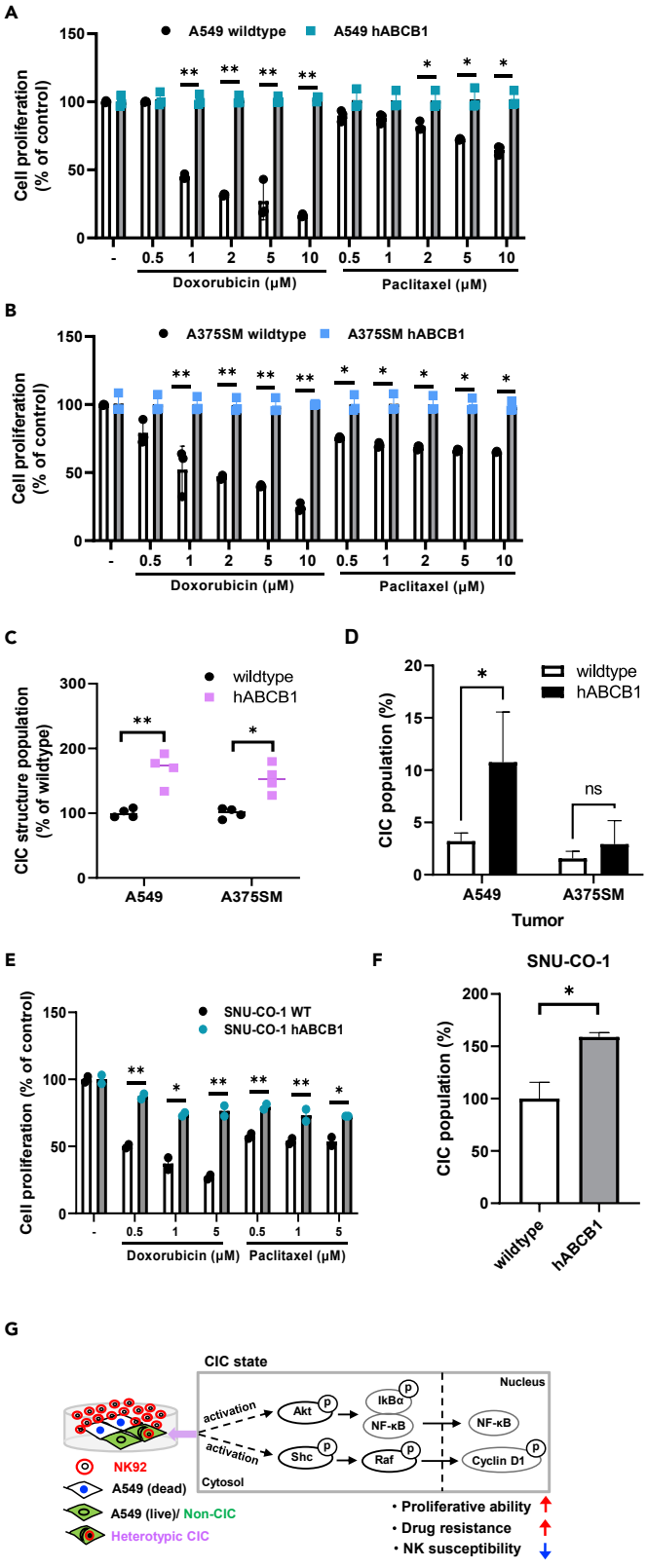
A
A549 wildtype
A549 hABCB1
Cell proliferation (% of control)
Doxorubicin (μM)
Paclitaxel (μM)
B
A375SM wildtype
A375SM hABCB1
C
wildtype
hABCB1
CIC structure population (% of wildtype)
A549
A375SM
D
CIC population (%)
ns
Tumor
E
SNU-CO-1 WT
SNU-CO-1 hABCB1
F
SNU-CO-1
G
CIC state
Nucleus
Cytosol
activation
Akt
IkBα
NF-κB
Shc
Raf
Cyclin D1
NK92
A549 (dead)
A549 (live)/ Non-CIC
Heterotypic CIC
• Proliferative ability
• Drug resistance
• NK susceptibility

Figure 7. Analysis of heterotypic CIC structures between hABCB1 overexpressing cancer and NK-92 cells

(A and B) Cell proliferation of wild-type or hABCB1 overexpressing A549 or A375SM cells was measured by CCK-8 assay after treatment with various concentrations of doxorubicin and paclitaxel (0.5, 1, 2, 5 and 10 μM) for 24 h. p values were determined using the student's *t*-tests. All experiments were performed in triplicate. *, $p<0.05$; **, $p<0.01$.

(C) A549 and A375SM wild-type or hABCB1 overexpressing cells were co-cultured with NK-92 cells for 4 h to analyze the heterotypic CIC population.

(D) Heterotypic CIC populations in NK-92 injected A549 and A375SM wild-type or hABCB1 overexpressing tumors of xenograft animal models were analyzed using flow cytometry. *, $p<0.05$; ns, not significant.

(E) Cell proliferation of wild-type or hABCB1 overexpressing cancer organoids (SNU-CO-1) were measured by CCK-8 assay after treatment with various concentrations of doxorubicin and paclitaxel (0.5, 1 and 5 μM) for 24 h. (F) The wild-type or hABCB1 overexpressing cancer organoids (SNU-CO-1) were co-cultured with NK-92 cells for 4 h to analyze the heterotypic CIC population.

(G) Heterotypic CIC and non-CIC formed by co-culture of A549 and NK-92 cells were isolated, and the differences in NK susceptibility and drug resistance were analyzed. The mechanistic model of this study is that the heterotypic CIC populations exhibit higher activation of signaling proteins such as Akt, IkBα, Shc, Raf and Cyclin D1, increased cancer cell growth and drug resistance, and decreased NK sensitivity compared to non-CIC populations.

The phosphor antibody array analysis confirmed that phosphorylation of signaling proteins such as Akt, Raf, IkBα, and Cyclin D1 is increased in heterotypic CIC-forming cancer cells compared to non-CIC (Figures 5D and 7G). Phosphorylation of cyclin D1 at Thr 286 during S phase is known to induce proteasome degradation, allow efficient DNA synthesis and promote cell cycle progression (Guo et al., 2005). Akt is well known as a master regulator of drug resistance, affecting cancer progression and immunosuppression, and interacting directly with the mitogen-activated protein (MAP) kinase signaling pathway (Kaboli et al., 2020). In addition, activation of proteins involved in anticancer drug target (Raf), cell membrane receptor-mediated signaling (SYK and Shc) and protein synthesis (4E-BP1) was confirmed (Figure 5D).

In conclusion, cancer cells that induce heterotypic CICs can be used as a functional biomarker to predict anticancer drug resistance and malignancy in the tumor microenvironment. Furthermore, depending on the proportion of the CIC population in the tumor tissue, we suggest this biomarker as a tool to predict the responsiveness of cell (NK or $CD8^+$ T) therapeutics and as a marker to determine whether a patient will develop resistance to anticancer chemotherapeutics.

Limitations of the study

A limitation of this study is that we were unable to interpret the cause of the difference between heterotypic CICs and non-CICs. Transcriptomic analysis was performed on cells isolated using a flow cytometry-based cell sorter, but no significant difference was found between the two populations (data not shown). To further clarify this point, it will be necessary to analyze extracellular ER miRNA, and genetic alterations. In addition, we would like to emphasize the need for single cell omics analyses in addition to bulk omics analyses because of tumor heterogeneity. To address this issue in the future, our laboratory is attempting to perform single cell isolation using laser microdissection equipment (Figure S5).

STAR★METHODS

Detailed methods are provided in the online version of this paper and include the following:

- KEY RESOURCES TABLE
- RESOURCE AVAILABILITY
  - Lead contact
  - Materials availability
  - Data and code availability
- METHOD DETAILS
  - Cell and organoid culture and treatment
  - Cellular imaging of heterotypic cell-in-cell structures (CICs) by laser scanning fluorescence microscopy and optical diffraction tomography
  - Analysis and cell sorting of heterotypic CICs by flow cytometry and cell sorter
  - Transmission electron microscopy (TEM) imaging
  - Calcein AM-based NK cytotoxicity
  - hABCB1 overexpressing cancer cells and organoids establishment
  - Assay of proliferative activity and drug resistance analysis

- Cell-cycle analysis
- Antibody array analysis
- Focus formation, anchorage independent growth, and invasion assay
- Flow cytometry analysis of epidermal growth factor receptor (EGFR) expression
- Cell sorting of heterotypic CIC by laser microdissection (LMD)
- *In vivo* heterotypic CIC analysis

● QUANTIFICATION AND STATISTICAL ANALYSIS

SUPPLEMENTAL INFORMATION

Supplemental information can be found online at https://doi.org/10.1016/j.isci.2022.105017.

ACKNOWLEDGMENTS

This work was supported by the National Research Foundation of Korea (NRF), through grants funded by the Korean Ministry of Science and Information Technology (MSIT) (No. NRF-2020R1C1C1012542), the National Research Council of Science & Technology (NST) (No.CAP-18-02-KRIBB and CCL22061-100), Korea Food Research Institute (No.E0210203), and Korea Basic Science Institute (No.K115000, C170100 and C170300). We acknowledge Dr. Yang Hoon Huh and Dr. Hyo Jung Kim at Korea Basic Science Institute (KBSI) for their contribution to technical assistant for TEM imaging and Dr. Su Min Lee at Tomocube for their contribution to technical assistant for optical diffraction tomography.

AUTHOR CONTRIBUTIONS

E.H.H. and K.S.H. conceived and designed the research. All authors contributed to the performance of cell-based experiments. Y-J.C. and E.H.H. performed cell-based imaging and flow cytometry analysis. H-J.K. performed ODT imaging and J.Y.M., S-Y.L., and J.K. analyzed the transcriptomic and proteomic data. E.H.H. drafted the manuscript, and all authors contributed to figure preparation. All authors approved the final manuscript.

DECLARATION OF INTERESTS

The authors declare no conflicts of interest or financial interests.

INCLUSION AND DIVERSITY

We worked to ensure diversity in experimental samples through the selection of the cell lines. The author list of this paper includes contributors from the location where the research was conducted who participated in the data collection, design, analysis, and/or interpretation of the work.

Received: January 12, 2022
Revised: July 13, 2022
Accepted: August 19, 2022
Published: September 16, 2022

REFERENCES

AbdullGaffar, B. (2020). Emperipolesis of lymphocytes by mesothelial cells in pleural effusion involved by T-lymphoblastic lymphoma. Diagn. Cytopathol. *48*, E22–E26.

Almangush, A., Mäkitie, A.A., Hagström, J., Haglund, C., Kowalski, L.P., Nieminen, P., Coletta, R.D., Salo, T., and Leivo, I. (2020). Cell-in-cell phenomenon associates with aggressive characteristics and cancer-related mortality in early oral tongue cancer. BMC Cancer *20*, 843.

Ahn, Y.H., Ren, L., Kim, S.M., Seo, S.H., Jung, C.R., Kim, D.S., Noh, J.Y., Lee, S.Y., Lee, H., Cho, M.Y., et al. (2020). A three-dimensional hyaluronic acid-based niche enhances the therapeutic efficacy of human natural killer cell-based cancer immunotherapy. Biomaterials *247*, 119960.

Caruso, R.A., Fedele, F., Finocchiaro, G., Arena, G., and Venuti, A. (2012). Neutrophil-tumor cell phagocytosis (cannibalism) in human tumors: an update and literature review. Exp. Oncol. *34*, 306–311.

Chen, Y.H., Wang, S., He, M.F., Wang, Y., Zhao, H., Zhu, H.Y., Yu, X.M., Ma, J., Che, X.J., Wang, J.F., et al. (2013). Prevalence of heterotypic tumor/immune cell-in-cell structure in vitro and in vivo leading to formation of aneuploidy. PLoS One *8*, e59418.

Fais, S., and Overholtzer, M. (2018). Cell-in-cell phenomena in cancer. Nat. Rev. Cancer *18*, 758–766.

Foulkes, W.D. (2007). p53–master and commander. N. Engl. J. Med. *357*, 2539–2541.

Gao, Y., Dorn, P., Liu, S., Deng, H., Hall, S.R.R., Peng, R.W., Schmid, R.A., and Marti, T.M. (2019). Cisplatin-resistant A549 non-small cell lung cancer cells can be identified by increased mitochondrial mass and are sensitive to pemetrexed treatment. Cancer Cell Int. *19*, 317.

Guo, Y., Yang, K., Harwalkar, J., Nye, J.M., Mason, D.R., Garrett, M.D., Hitomi, M., and Stacey, D.W. (2005). Phosphorylation of cyclin D1 at Thr 286 during S phase leads to its proteasomal degradation and allows efficient DNA synthesis. Oncogene *24*, 2599–2612.

Hamann, J.C., Kim, S.E., and Overholtzer, M. (2019). Methods for the study of entotic cell death. Methods Mol. Biol. *1880*, 447–454.

Hayashi, A., Yavas, A., McIntyre, C.A., Ho, Y.J., Erakky, A., Wong, W., Varghese, A.M., Melchor, J.P., Overholtzer, M., O'Reilly, E.M., et al. (2020). Genetic and clinical correlates of entosis in pancreatic ductal adenocarcinoma. Mod. Pathol. *33*, 1822–1831.

He, M., Huang, H., Wang, M., Chen, A., Ning, X., Yu, K., Li, Q., Li, W., Ma, L., Chen, Z., et al. (2015). Fluorescence-activated cell sorting analysis of heterotypic cell-in-cell structures. Sci. Rep. *5*, 9588.

Huang, H., Chen, A., Wang, T., Wang, M., Ning, X., He, M., Hu, Y., Yuan, L., Li, S., Wang, Q., et al. (2015a). Detecting cell-in-cell structures in human tumor samples by E-cadherin/CD68/CD45 triple staining. Oncotarget *6*, 20278–20287.

Huang, H., Chen, Z., and Sun, Q. (2015b). Mammalian cell competitions, cell-in-cell Phenomena and their biomedical implications. Curr. Mol. Med. *15*, 852–860.

Huang, H., He, M., Zhang, Y., Li, W., Cui, P., Wang, X., Zhang, B., Niu, Z., Zheng, Y., Sun, Q., et al. (2020). Identification and validation of heterotypic cell-in-cell structure as an adverse prognostic predictor for young patients of resectable pancreatic ductal adenocarcinoma. Signal Transduct. Target.Ther. *5*, 246.

Ichite, N., Chougule, M.B., Jackson, T., Fulzele, S.V., Safe, S., and Singh, M. (2009). Enhancement of docetaxel anticancer activity by a novel diindolylmethane compound in human non-small cell lung cancer. Clin. Cancer Res. *15*, 543–552.

Jabbarzadeh Kaboli, P., Salimian, F., Aghapour, S., Xiang, S., Zhao, Q., Li, M., Wu, X., Du, F., Zhao, Y., Shen, J., et al. (2020). Akt-targeted therapy as a promising strategy to overcome drug resistance in breast cancer - a comprehensive review from chemotherapy to immunotherapy. Pharmacol. Res. *156*, 104806.

Lee, S.H., Yun, S., Piao, Z.H., Jeong, M., Kim, D.O., Jung, H., Lee, J., Kim, M.J., Kim, M.S., Chung, J.W., et al. (2010). Suppressor of cytokine signaling 2 Regulates IL-15–Primed human NK cell function via control of phosphorylated Pyk2. J. Immunol. *185*, 917–928.

Mackay, H.L., Moore, D., Hall, C., Birkbak, N.J., Jamal-Hanjani, M., Karim, S.A., Phatak, V.M., Piñon, L., Morton, J.P., Swanton, C., et al. (2018). Genomic instability in mutant p53 cancer cells upon entotic engulfment. Nat. Commun. *9*, 3540.

Onishi, T., Tazawa, H., Hashimoto, Y., Takeuchi, M., Otani, T., Nakamura, S., Sakurai, F., Mizuguchi, H., Kishimoto, H., Umeda, Y., et al. (2016). Tumor-specific delivery of biologics by a novel T-cell line HOZOT. Sci. Rep. *6*, 38060.

Overholtzer, M., and Wang, X. (2015). Cell-in-Cell: a century-old mystery comes to the table. Curr. Mol. Med. *15*, 802–804.

Jeevitha Priya, M., Vidyalakshmi, S., and Rajeswari, M. (2022). Study on reversal of ABCB1 mediated multidrug resistance in Colon cancer by acetogenins: an *in- silico* approach. J. Biomol. Struct.Dyn. *40*, 4273–4284.

Ruan, B., Niu, Z., Jiang, X., Li, Z., Tai, Y., Huang, H., and Sun, Q. (2019). High frequency of cell-in-cell formation in heterogeneous human breast cancer tissue in a patient with poor prognosis: a case report and literature review. Front. Oncol. *9*, 1444.

Schenker, H., Büttner-Herold, M., Fietkau, R., and Distel, L.V. (2017). Cell-in-cell structures are more potent predictors of outcome than senescence or apoptosis in head and neck squamous cell carcinomas. Radiat.Oncol. *12*, 21.

Sierro, F., Tay, S.S., Warren, A., Le Couteur, D.G., McCaughan, G.W., Bowen, D.G., and Bertolino, P. (2015). Suicidal emperipolesis: a process leading to cell-in-cell structures, T cell clearance and immune homeostasis. Curr. Mol. Med. *15*, 819–827.

Stewart, D.J. (2010). Tumor and host factors that may limit efficacy of chemotherapy in non-small cell and small cell lung cancer. Crit. Rev. Oncol. Hematol. *75*, 173–234.

Tetsu, O., Hangauer, M.J., Phuchareon, J., Eisele, D.W., and McCormick, F. (2016). Drug resistance to EGFR inhibitors in lung cancer. Chemotherapy *61*, 223–235.

Vasan, N., Baselga, J., and Hyman, D.M. (2019). A view on drug resistance in cancer. Nature *575*, 299–309.

Wang, M., Niu, Z., Qin, H., Ruan, B., Zheng, Y., Ning, X., Gu, S., Gao, L., Chen, Z., Wang, X., et al. (2020). Mechanical ring interfaces between adherens junction and contractile actomyosin to coordinate entotic cell-in-cell formation. Cell Rep. *32*, 108071.

Wang, X., Li, Y., Li, J., Li, L., Zhu, H., Chen, H., Kong, R., Wang, G., Wang, Y., Hu, J., and Sun, B. (2019). Cell-in-cell phenomenon and its relationship with tumor microenvironment and tumor porogression: a review. Front. Cell Dev. Biol. *7*, 311.

Wang, Y., and Wang, X.N. (2013). Cell-in-cell: a virgin land of cell biology. OncoImmunology *2*, e25988.

Zhang, H., Wang, Y., Liu, X., and Li, Y. (2020). Progress of long noncoding RNAs in anti-tumor resistance. Pathol. Res. Pract. *216*, 153215.

Zhang, X., Niu, Z., Qin, H., Fan, J., Wang, M., Zhang, B., Zheng, Y., Gao, L., Chen, Z., Tai, Y., et al. (2019). Subtype-based prognostic analysis of cell-in-cell structures in early breast cancer. Front. Oncol. *9*, 895.

STAR★METHODS

KEY RESOURCES TABLE

REAGENT or RESOURCE	SOURCE	IDENTIFIER
Antibodies		
CD45-PE	Beckman Coulter	Cat# A07783
Alexa Fluor 647-conjugated anti-EGF Receptor	BD Biosciences	Cat# 558523; RRID: AB_647124
Alexa Fluor 488-conjugated anti-CD324 (E-cadherin)	Thermo Fisher Scientific, Invitrogen, eBioscience	Cat# 53-3249-82; RRID: AB_10671003
Bacterial and virus strains		
pLV[Exp]-Puro-EF1A-hABCB1 [NM_001348945.1]	Vectorbuilder	ID: VB900100-2568gcj
Chemicals, peptides, and recombinant proteins		
CellTracker™ Green CMFDA (5-chloromethylfluorescein diacetate)	Thermo Fisher Scientific, Invitrogen	Cat# C7025
CellTrace™ Calcein Green, AM	Thermo Fisher Scientific, Invitrogen	Cat# C34852
CellTrace™ Calcein Red-orange, AM	Thermo Fisher Scientific, Invitrogen	Cat# C3100MP
SYTOX™ Blue Dead Cell Stain	Thermo Fisher Scientific, Invitrogen	Cat# S34857
Etoposide	Sigma-Aldrich, Merck	Cat# E1383
Doxorubicin	Sigma-Aldrich, Merck	Cat# D1515
Gemcitabine hydrochloride	Sigma-Aldrich, Merck	Cat# G6423
Cisplatin	Sigma-Aldrich, Merck	Cat# PHR1624
Paclitaxel	Sigma-Aldrich, Merck	Cat# T7402
D-myo-inositol	Sigma-Aldrich, Merck	Cat# I9766
2-mercaptoethanol	Gibco	Cat# 21985023
folic acid	Sigma-Aldrich, Merck	Cat# F7876
Recombinant IL-2	Pepro Tech	Cat# 200–02
Human EGF	R&D Systems	236-EG-200
Human FGF-10	R&D Systems	Cat# 345-FG-025
Nicotinamide	Sigma-Aldrich, Merck	Cat# N3376
N-acetylcysteine	Sigma-Aldrich, Merck	Cat# A7250
A83-01	Sigma-aldrich	Cat# SML0788
SB202190	Tocris	Cat# 1614
prostaglandin E2	STEMCELL Technologies	Cat# 72192
N2 supplement	Invitrogen	Cat# 17502048
Triton X-100	Sigma-Aldrich, Merck	Cat# X100
Hoechst 33342	Thermo Fisher Scientific, Invitrogen	Cat# H3570
RBC Lysing buffer Hybrid-Max	Sigma-Aldrich	Cat# R7757
Per-Fix nc kit	Beckman Coulter	Cat# B10825
Rhodamine 123	Sigma-Aldrich, Merck	Cat# R8004
crystal violet	Sigma-Aldrich, Merck	Cat# C3886
Critical commercial assays		
Cell counting kit-8	Dojindo Laboratories	Cat# CK04
Cell Signaling Phospho Antibody Array	Fullmoon Biosystems	Cat # PCS300
Experimental models: Cell lines		
NK-92	Laboratory of Tae Don Kim (Ahn et al., 2020)	N/A
A549	Laboratory of Tae Don Kim (Lee et al., 2010)	N/A

(*Continued on next page*)

Continued

REAGENT or RESOURCE	SOURCE	IDENTIFIER
A431	Laboratory of Tae Don Kim	N/A
PLC/PRF/5	Laboratory of Tae Don Kim	N/A
A375SM	Korea Cell Line Bank	Cat# 80004
SNU-1-CO cancer organoids	Korea Cell Line Bank	Cat# 00001-CO
Experimental models: Organisms/strains		
Mouse: SCID	RaonBio Inc.	Strain name: NOD.CB17-Prkdc$^{scid/scid}$/Rj
Software and algorithms		
Ingenuity pathway analysis	Qiagen, Ingenuity systems	https://digitalinsights.qiagen.com
Graphpad prism 9	Graphpad software	https://www.graphpad.com/scientific-software/prism/

RESOURCE AVAILABILITY

Lead contact

Further information should be directed to and will be fulfilled by the lead contact Dr. Eun Hee Han (heh4285@kbsi.re.kr).

Materials availability

This study did not generate new unique materials or reagents.

Data and code availability

All data produced or analyzed for this study (including video files) are included in the published article and its supplemental information files. This study did not generate any code. Any additional information required to reanalyze the data reported in this paper is available from the lead contacton request.

METHOD DETAILS

Cell and organoid culture and treatment

The NK-92 (human natural killer cell line), A549 (human non-small cell lung cancer cell line), and EGFR-over-expressed A431 (human skin cancer cell line), and PLC/PRF/5 (human liver hepatoma cancer cell line) cells were kindly gifted from Dr. Tae Don Kim (Korea Research Institute Bioscience and Biotechnology, South Korea). The A375SM (human melanoma) cell line and cancer organoids (SNU-1-CO) are obtained from Korea Cell Line Bank (KCLB, Seoul, Republic of Korea). The NK-92 cells were grown in alpha minimum essential medium with 12.5% fetal bovine serum (FBS) and 12.5% horse serum. To prepare the complete growth medium, the following components were added to the base medium before use: 0.2 mM inositol, 0.1 mM 2-mercaptoethanol, 0.02 mM folic acid, and 200 U/mL recombinant IL-2 (Cat. 200–02, Peprotech, Rocky Hill, NJ, USA). Other cells were cultured in Dulbecco's modified Eagle's medium (DMEM) (A549), Eagle's Minimum Essential Medium (EMEM) (PLC/PRF/5, A375SM) or RPMI-1640 (A431) supplemented with 10% FBS in a humidified 5% CO_2 incubator at 37°C. Cancer organoids were cultured in 40% w/v DMEM/F12 supplemented with 50% w/v L-WRN conditioned medium, 1 x B27, 50 ng/mL human EGF, 10 ng/mL human FGF-10, 10 mM nicotinamide, 1.25 mM N-acetylcysteine, 500 nM A83-01, 3 μM SB202190, 10 nM prostaglandin E2, N2 supplement in a humidified 5% CO_2 incubator at 37°C. Stock solutions of anticancer drugs were prepared in dimethylsulfoxide (DMSO) and were added directly to the culture media. The control cells were treated only with DMSO, and the final DMSO concentration was always <0.2%.

Cellular imaging of heterotypic cell-in-cell structures (CICs) by laser scanning fluorescence microscopy and optical diffraction tomography

Time-lapse microscopic imaging was performed as follows. Calcein green AM and red-orange AM (Thermo Fisher Scientific, Waltham, MA, USA), with excitation/emission wavelengths of 480/515 nm and 577/590nm, respectively, were diluted in PBS or DMSO at a concentration of 1mg/mL and applied to cells for 30min. Target A549 cells were grown as monolayer on confocal slides (Ibidi, Munich, Germany) overnight, and stained with calcein green AM. Subsequently, NK-92 cells stained with calcein red-orange AM were added

to the culture dish. The cells were then visualized with the LSM710 laser scanning confocal microscope (Carl Zeiss, Oberkochen, Germany). Cells were maintained under conditions of 37°C and 5% CO_2. A549 and NK cells were tracked and analyzed using Zen software (Carl Zeiss). For optical diffraction tomography study, A549 cells were cultured in a Tomodish (Tomocube, Daejeon, Korea) and co-cultured with NK-92 cells for several time periods (0, 20, 40 and 60 min). The cells were washed twice with D-PBS, and then the buffer was replaced with culture medium. A commercial microscope (HT-2H, Tomocube) was used to image heterotypic CIC formation. Images of a three-dimensional (3D) refractive index (RI) distribution were rendered using Tomostudio (HT-2H, Tomocube).

Analysis and cell sorting of heterotypic CICs by flow cytometry and cell sorter

Live NK-92 cells were stained with a specific surface marker (CD45) by incubation in PBS with 1% FBS containing CD45-PE antibody (Cat. A07783; Beckman Coulter, Brea, CA, USA) for 15 min prior to co-culture. Target cancer cells were grown on a 6-well plate to adhere overnight and then stained with CMFDA cell tracker (Thermo Fisher Scientific) for 20 min. Afterwards, cells were co-cultured for 4 h, and then washed with PBS and harvested using a trypsin/EDTA solution. Cells were pelleted at 1000 rpm for 2 min and re-suspended in 400 μL PBS supplemented with 0.5% FBS. Heterotypic CIC populations were then analyzed by flow cytometry (CytoFlex, Beckman Coulter) and sorted by a cell sorter (Astrios, Beckman Coulter) installed with Kaluza software (Beckman Coulter, USA). Heterotypic CIC populations were calculated as reported (He et al., 2015) using the equation: heterotypic CICs (%) = (double-positive cells in quadrant right-high/single-positive tumor cells in quadrant right-low) × 100.

Transmission electron microscopy (TEM) imaging

Co-cultured A549 and NK cells were fixed in 2% glutaraldehyde and 2% paraformaldehyde in 0.1 M phosphate buffer (pH 7.4) for 2 h at 4°C. After washing three times with PBS, the cells were fixed in 1% osmium tetroxide on ice for 2 h and washed again three times. The cells were then embedded in Epon 812 (Salt Lake City, UT, USA) after dehydration in a series of ethanol and propylene oxide. Polymerization was conducted with pure resin at 70°C for 24 h. Ultrathin sections (~70 nm) were obtained with a model MT-X ultramicrotome (RMC, Tucson, AZ, USA) and collected on 100 mesh copper grids. After staining with uranyl acetate and lead citrate, the sections were visualized using a JEM-1400 Plus Bio-HVEM System Plus at 120 kV and a JEM-1000BEF at 1000 kV (Jeol, Tokyo, Japan).

Calcein AM-based NK cytotoxicity

NK cell cytotoxicity was measured with calcein AM release assay. Target cancer cells were labeled with calcein green (Thermo Fisher Scientific) for 30minat 37°C. The labeled cancer cells (1×10^4 cells) and serially diluted effector cells (E:T = 2:1, 4:1, 6:1, and 8:1) were then co-cultured on 96-well round-bottom plates for 4 h. Calcein released into the supernatant was measured using a multimode microplate reader (Spectra Max M5, Molecular Device Co. San Jose, CA, USA). Maximum release was simulated based on the addition of 1% Triton X-100 (Sigma, St. Louis, MO, USA) to the target cells, and spontaneous release was simulated by adding culture media to the target cells. The percentage of specific lysis was calculated according to the following formula: (sample release – spontaneous release)/(maximum release – spontaneous release) × 100.

hABCB1 overexpressing cancer cells and organoids establishment

Cells (A549 and A375SM; 50,000 cells per well) and cancer organoids (SNU-1-CO; 20,000 cells per well) were seeded in 24 well plates. After 24 h, cells were infected hABCB1 lentivirus particle (pLV[Exp]-Puro-EF1A-hABCB1 [NM_001348945.1] from Vectorbuilder, vector ID: VB900100-2568gcj) using a Trans-Dux MAX reagent (Systembio) and they were treated with puromycin 1 μg/mL for 2 weeks. To investigate hABCB1 overexpressing, rhodamine 123 accumulation was detected by cellular imaging and flow cytometry. Cells and cancer organoids were treated with rhodamine 123 (5 μM, Sigma-Aldrich; #83702) for 30 min in CO_2 incubator. After washed with PBS, cellular images were captured by confocal microscopy (LSM 710, Carl Zeiss) and cellular nuclei were stained with DAPI. Cellular fluorescence intensity was identified by flow cytometry (CytoFlex, Beckman Coulter).

Assay of proliferative activity and drug resistance analysis

Cells were seeded in 96-well plates (50,000 cells per well) and treated with various concentrations of anticancer reagents (docetaxel, etoposide, doxorubicin, and gemcitabine) for the desired time. Cell viability and cytotoxicity were measured by cell counting kit-8 assay (CCK-8, Dojindo, Japan), according to the

recommended guidelines. 10 μL of CCK-8 was added into each well and incubated with cells for 1–4 h. The absorbance was measured on a microplate reader (Spectra Max M5, Molecular Device Co. San Jose, CA, USA) at 450 nm. Cell viability and cytotoxicity were obtained by measuring the absorbance intensity of anticancer drug (cisplatin, doxorubicin, gemcitabine, etoposide, and docetaxel)-treated cells compared to that of control cells (DMSO treatment). For drug resistance analysis, wild-type or ABCB1 overexpressing cancer cells and cancer organoids were treated with anticancer drugs, including doxorubicin (0.5–10 μM) and paclitaxel (0.5–10 μM).

Cell-cycle analysis

Cell cycling was determined using Hoechst 33342 (Thermo Fisher Scientific) according to the manufacturer's instructions. The cells were trypsinized and harvested by centrifugation, washed once with a D-PBS and stained with Hoechst 33342 in the dark at room temperature for 30 min. Finally, the cells were analyzed by flow cytometer (MoFlo Astrios, Beckman Coulter) and cell cycle distributions were calculated using Kaluza software (Version 2.1, Beckman Coulter).

Antibody array analysis

To investigate the differential protein expression of CIC vs non-CIC, analysis was performed using a Cell Signaling Phospho Antibody Array (PCS300, Fullmoon Biosystems, Sunnyvale, CA, USA) in e-biogen (Seoul, Republic of Korea), following one of the typical methods of analysis in e-biogen. Whole cell lysates were extracted by RIPA buffer containing protease and phosphatase inhibitor cocktail (Sigma-Aldrich, St. Louis, MO, USA). After protein extraction, glass slides for microarrays were incubated on a shaking incubator for 45 min after coating with 304 of total or phospho antibodies. After treatment with a blocking solution, the slides were thoroughly washed with distilled water, after which bound-biotinylated proteins were detected using Cy3-labeled streptavidin (1:1000 dilution, GE Healthcare, Little Chalfont, UK). After 20 min of incubation, the slides were washed, completely dried, and then scanned with a GenePix 4100A scanner (Molecular Devices, Sunnyvale, CA, USA). The scanned images were quantified using GenePix 7.0 software (Molecular Devices).

Focus formation, anchorage independent growth, and invasion assay

500 and 1000 sorted cells defined as heterotypic CICs or non-CICs, respectively, were seeded into 6 well plates and cultured for 8 days to allow foci formation. After incubation, the cells were washed in PBS and stained with 0.1% crystal violet (Amersco, Solon, OH, USA) in 50% methanol for counting. For the soft agar anchorage independent growth assay, the cells were trypsinized to generate single-cell suspensions and counted. 1.2% agarose (Promega, Madison, WI, USA) dissolved in medium was plated at the bottom of each well in a 12-well plate with an ultra-low adhesion surface. Briefly, single cell suspensions (5×10^4 and 1×10^5 cells per well) were mixed with 0.6% agarose and seeded on top of the agar. The cells were incubated at 37°C for 3 weeks to allow colony formation. Images were captured using an inverted wide field microscope (Axio Vert.A1, Carl Zeiss, Oberkochen, Germany) equipped with a G12 camera (Canon, Tokyo, Japan). Cells were sorted according to the presence or absence of heterotypic CIC formation were seeded into a matrigel-coated invasion chamber (Corning Incorporated, Corning, NY, USA). Briefly, the cells were seeded into an insert chamber with FBS-free media and cultured in 24-well plates supplemented with complete media for appropriate time period, then fixed with 4% formaldehyde and stained with crystal violet. The stained cells were observed under a microscope and the absorbance of the migrated cells was measured. All assays were performed in triplicate.

Flow cytometry analysis of epidermal growth factor receptor (EGFR) expression

PLC/PRF/5 and A431 cell monolayers were mobilized with trypsin/EDTA solution (Invitrogen) and re-suspended at a density of 2×10^7 cells/mL. The cells (10^6) were stained with Alexa Fluor 647-conjugated anti-EGFR (clone EGFR.1; BD Biosciences, San Jose, CA, USA) and analyzed on a flow cytometry (CytoFlex, Beckman Coulter) using Kaluza software. Live cells were identified by gating for forward scatter/side scatter.

Cell sorting of heterotypic CIC by laser microdissection (LMD)

Laser capture microdissection (LCM) was used to separate heterotypic CIC from cancer and NK-92 co-culture condition. Approximately 1000 cells from co-culture system were captured on a thermoplastic film using the laser microdissection system (LMD 6, Leica, Germany). The laser micro-dissected heterotypic

CIC-inducing cells were dropped by gravity into 0.2 mL PCR tube cap and stored at −80°C before the next analysis such as transcriptomics.

In vivo heterotypic CIC analysis

Animal experiments complied with the guidelines of the Institutional Animal Care and Use Committee (KBSI-IACUC-22-12) of the Korea Basic Science Institute (KBSI). SCID (male, 6 weeks old) mice were purchased from RaonBio Inc. (Yongin, Republic of Korea). For this experiment, 1 X 10^6 cells of wild-type and hABCB1-overexpressed A549 and A375SM cancer cells were simultaneously injected into the lower left or right flanks of SCID mice (3 per group). After waiting at least 3 weeks for the tumor to grow, NK-92 cells (5 X 10^6) were injected intratumorally. After 1 day, the tumors were isolated to make single cells, and the remaining cells in which red blood cells were lysed (RBC Lysing buffer Hybrid-Max, Sigma-Aldrich, #R7757) were permeabilized and fixed using a Per-Fix nc kit (Beckman Coulter, #B10825). Heterotypic CIC was counted by flow cytometry using CD324 (E-cadherin, eBioscience, #53-3249-82) and CD45-PE antibodies.

QUANTIFICATION AND STATISTICAL ANALYSIS

GraphPad Prism 9.4.1 was used to collect and analyze data. All data are expressed as the mean ± standard error of the mean (S.E.M.). Statistical analysis was performed using Student's t-test and Mann-Whitney U-test when the data did not follow a normal distribution. Statistical significance was set at $p<0.05$. We did not exclude samples or animals. No statistical methods were used to predetermine sample sizes, but our sample sizes are like those generally employed in the field.